Fibonacci Quasicrystals of Transmission-Line Resonators

Author: Benjamin Moy

Advisor: Jens Koch

Senior Honors Thesis

Department of Physics and Astronomy

Northwestern University

Evanston, IL 60208 USA

May, 2018

Abstract

We study a new artificial Fibonacci quasicrystal constructed of transmission-line resonators. We develop the mathematical formalism for describing such a quasicrystal and then use it to perform numerical calculations for two types of quasicrystals. One type, with varying impedances, displays the self-similarity that is characteristic of a quasicrystal. However, in the other type, where the wave speeds vary while impedances are constant, most typical properties of quasicrystals are destroyed. To understand why the usual quasicrystal properties do not persist, we extend the Kohmoto-Kadanoff-Tang (KKT) renormalization-group method. Finally, we present an invariant associated with this renormalization-group method.

Acknowledgments

First and foremost, I would like to thank my research advisor, Professor Jens Koch, for helping me grow as a physicist and for introducing me to quasicrystals. Jens always tries to develop physical intuition when I show him results, which is something I will take with me to graduate school. I would also like to thank Professor Anupam Garg for his many insights and for teaching me about past work on quasicrystals. In particular, Anupam suggested working through the original paper on the Kohmoto-Kadanoff-Tang (KKT) renormalization-group method, which is a key part of this thesis. In meeting with Jens and Anupam regularly, I have learned a lot about physics and about how to approach research problems.

In addition, I credit Dr. Andy Li with teaching me about transmission-line resonators. I also acknowledge Professor Bill Halperin and Andrew Zimmerman for originally starting me in research.

The research in this work was supported by a WCAS Summer Grant.

Contents

Chapter 1

Introduction

1.1 What is a Quasicrystal?

Crystals are highly-ordered materials in which the constituents are arranged periodically. This results in periodic eigenmodes of phonons and electrons that extend across the entire crystal. In contrast, disordered solids have constituents that are arranged randomly and have localized high-frequency phonon eigenmodes and high-energy electronic wave functions. This, then, raises the question: Is there a kind of material in between a crystal and a disordered solid? The answer is yes. Quasicrystalline lattices are geometric configurations of building blocks that are ordered but do not repeat periodically and can exhibit symmetries and other properties that are prohibited in conventional crystals. While quasicrystals do not have translational symmetry, they can display new rotational symmetries (Figure 1.1). For example, ordinary crystals cannot have five-fold rotational symmetry for the same reason that a bathroom floor cannot be completely covered with only pentagonal tiles. But fascinatingly enough, quasicrystals can in fact have five-fold rotational symmetry [2]. Quasicrystals have a host of other intriguing mathematical characteristics that include sets of energy levels that are neither discrete nor continuous as well as wave functions with fractal properties [3]. In recent work, physicists have also established a connection between quasicrystals

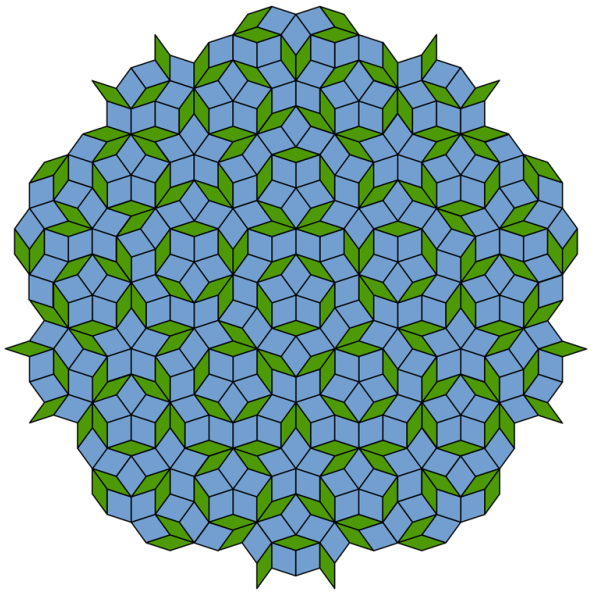

Figure 1.1: Penrose tiling. The Penrose tiling is an example of a two-dimensional quasicrystal with five-fold rotational symmetry [1].

and topological properties of quantum Hall systems [4, 5]. A new platform of investigating quasicrystals that is driving modern research is artificial quasicrystal systems, including realizations in ultra-cold atoms in optical lattices [6] and photonic waveguide arrays [7]. In this thesis, we study a new artificial quasicrystal system constructed of transmission-line resonators. For this system, we consider two types of quasicrystals. One type displays the usual self-similarity of a quasicrystal, but in the other type, most of the typical properties of quasicrystals turn out to be absent.

Like in a crystal, there is a set of rules for the arrangement of the constituents of a quasicrystal, resulting in the highly ordered and symmetric structure of the material. In this thesis, we focus on the Fibonacci quasicrystal, a one-dimensional quasicrystal composed of two basic units, which we will call L and S. To generate the pattern of L's and S's that form the Fibonacci quasicrystal, we start with a single-element list of either L or S and then use the substitution rules $L \to LS$ and $S \to L$ to generate a new list. We can iteratively continue

this process, and the resulting pattern of L's and S's define a Fibonacci quasicrystal:

Step 1: S

Step 2: L

Step 3: LS

Step 4: LSL

Step 5: $LSLLS$

Step 6: $LSLLSLSL$

Step 7: $LSLLSLSLLSLLS$

$\vdots$

This type of quasicrystal is called a Fibonacci quasicrystal because the chain in the nth step may be constructed by adding the $(n-2)$th iteration to the end of the $(n-1)$th iteration. This is similar to the Fibonacci sequences of numbers since the nth Fibonacci number F_n is given by $F_n = F_{n-1} + F_{n-2}$. Moreover, the number of elements in each iteration of the Fibonacci quasicrystal chain follows the Fibonacci sequence.

1.2 Properties of Quasicrystals

A physical example of a Fibonacci quasicrystal is a one-dimensional chain of coupled oscillators with identical springs in which two types of masses vary according to the pattern of L's and S's. In general, the matrix equation to solve for the eigenmodes and eigenfrequencies is

a generalized eigenvalue problem of the form

$$\omega^2 \begin{pmatrix} m_1 & & & & \\ & m_2 & & & \\ & & m_3 & & \\ & & & \ddots & \\ & & & & m_N \end{pmatrix} \begin{pmatrix} x_1 \\ x_2 \\ x_3 \\ \vdots \\ x_N \end{pmatrix} = k \begin{pmatrix} 2 & -1 & & & \\ -1 & 2 & -1 & & \\ & -1 & \ddots & \ddots & \\ & & \ddots & \ddots & -1 \\ & & & -1 & 2 \end{pmatrix} \begin{pmatrix} x_1 \\ x_2 \\ x_3 \\ \vdots \\ x_N \end{pmatrix} \tag{1.1}$$

where x_n is the displacement from equilibrium of point mass m_n, k is the spring constant of each spring, N is the number of masses, and ω is an eigenfrequency. (We have imposed hard-wall boundary conditions.) The two types of masses vary in the pattern of the Fibonacci quasicrystal. As an example, we examine the eigenfrequency spectrum and some eigenvectors for the case in which $m_2/m_1 = 4$ and $N = 1597$.

If all eigenfrequencies are ordered in a list from least to greatest, then the eigenmode number is defined as the position of the given eigenfrequency in this list. The eigenfrequency spectrum displays self-similarity, as depicted in Figure 1.2. The right figure shows that the top "band" of the left figure actually looks like the top three "bands" in the same figure. Hence, these "bands" are not actually bands at all since they are not continuous.

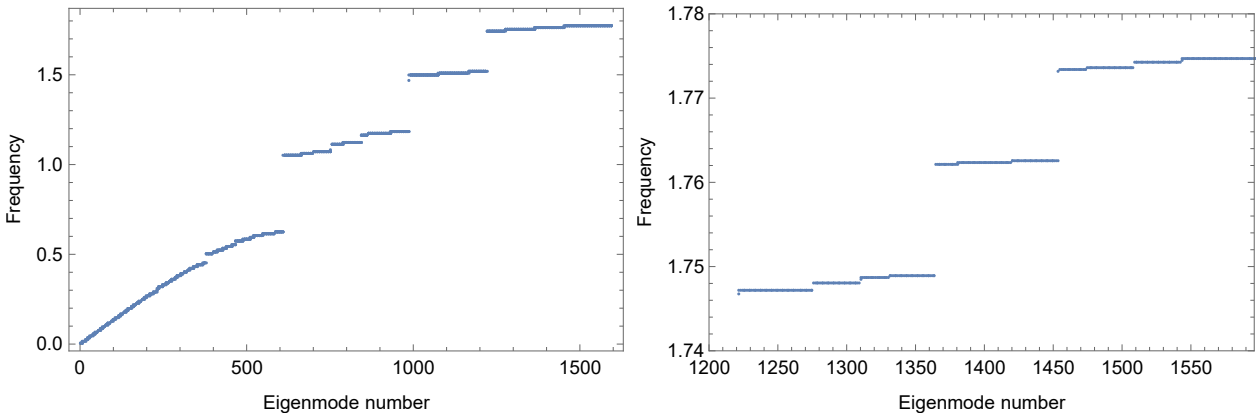

Figure 1.2: Eigenfrequency spectrum. The left plot depicts all eigenfrequencies (in units of $\sqrt{k/m_1}$) ordered from least to greatest. The right plot shows the eigenfrequencies from eigenmode number 1200 to eigenmode number 1597, the eigenfrequencies in the top "band" of the left figure. By comparing the two plots, we see the self-similarity of the eigenfrequency spectrum.

Some of the high-frequency eigenmodes are shown in Figure 1.3. While their corresponding eigenvalues appear to be the same from numerical calculations, this eigenvalue is not degenerate. There is a change of coordinates that makes solving Eq. (1.1) equivalent to computing the eigenvectors and eigenvalues of a tridiagonal real-symmetric matrix. Such a matrix cannot have any degeneracies due to a theorem in linear algebra [8].

The high-frequency modes have some localized portions, but they are not completely localized modes like in a disordered chain. In addition, all these high-frequency eigenmodes have some fractal structure as well. To make this characteristic more apparent, Figure 1.4 shows a portion of the highest frequency mode that looks similar to the full plot of the eigenmode.

The lower-frequency eigenmodes are delocalized and do not display this self-similarity. The eigenmodes of the lowest possible eigenfrequencies in the spectrum look like sinusoidal waves, just as they do for both crystals and disordered chains.

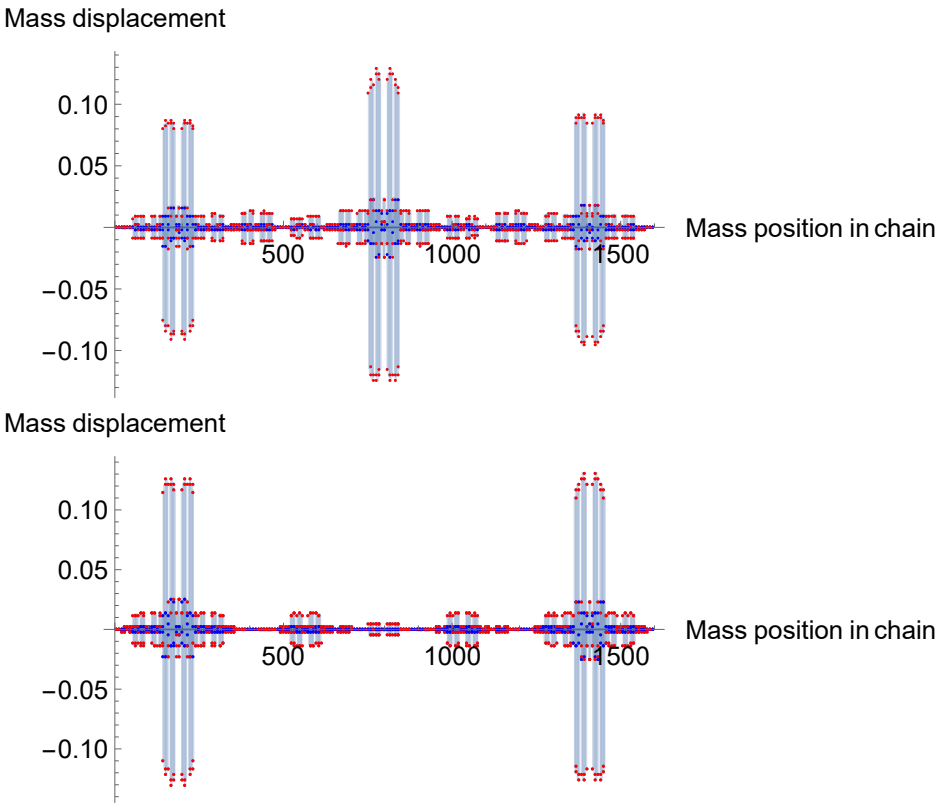

Figure 1.3: The third and fourth highest frequency eigenmodes, respectively. Both have eigenfrequency close to 3.14968. Red points correspond to the lighter masses in the chain while blue points correspond to the heavier masses.

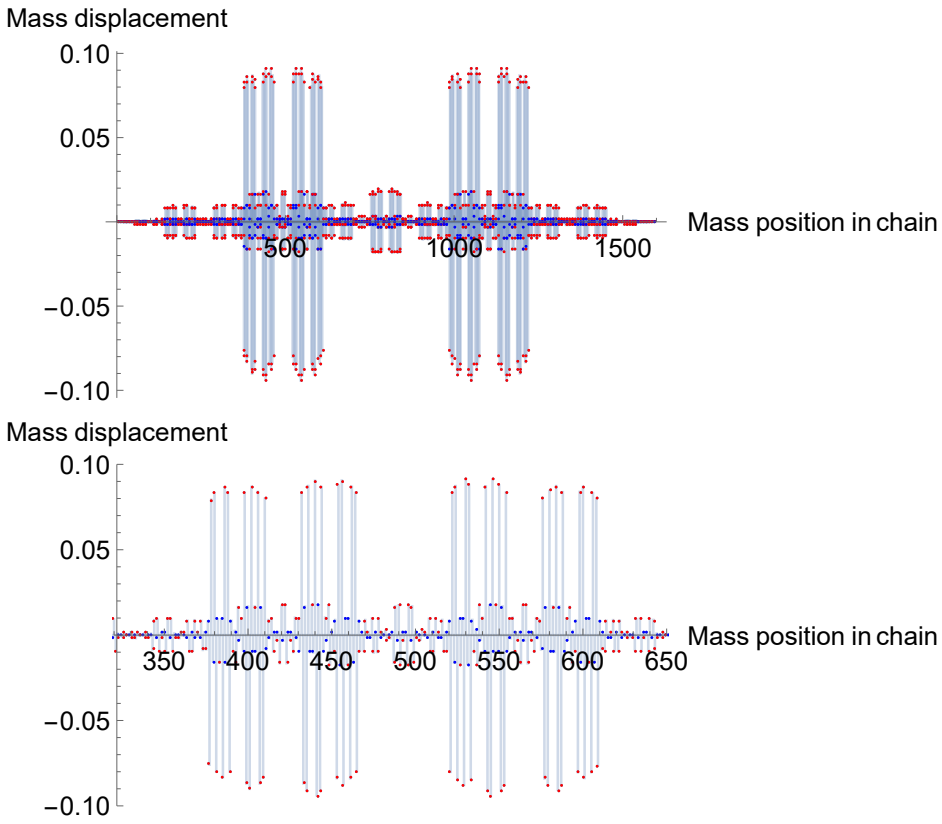

Figure 1.4: Highest frequency eigenmode, which has eigenfrequency $\omega = 3.14968$. The top plot depicts the full eigenmode while the bottom plot shows from mass position 320 to 650. The similarity of these images indicates that this eigenmode has a self-similar structure.

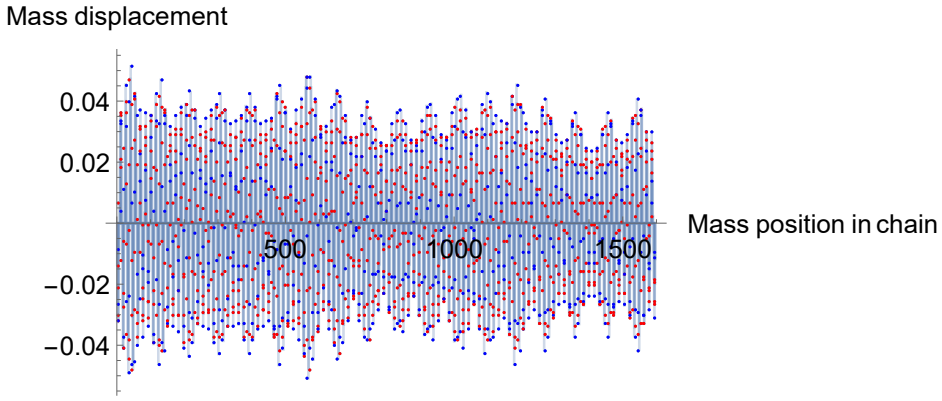

Figure 1.5: Eigenmode with eigenfrequency 0.078804. This low-frequency eigenmode is delocalized and does not display self-similarity.

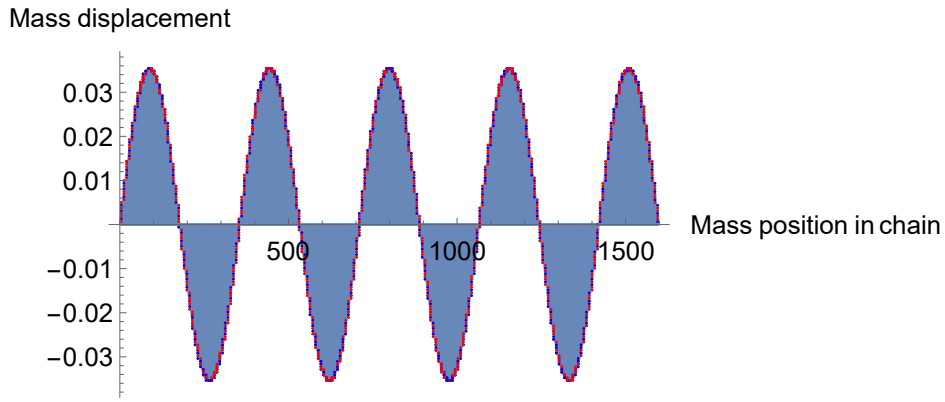

Figure 1.6: Eigenmode with eigenfrequency 0.00014587. This eigenmode has the ninth lowest eigenfrequency and looks like a sinusoidal wave.

Chapter 2

Transmission-Line Resonators

2.1 Equations of Motion and Boundary Conditions

Recently, there have been many efforts to build new simulations of quantum matter in circuit quantum electrodynamics (circuit QED) lattices due to their flexibility in fabrication and their easy accessibility to non-equilibrium physics [9]. In this thesis, we are interested in studying the physics of Fibonacci quasicrystals realized by transmission-line resonators, which are elements of circuit QED lattices. Before discussing the Fibonacci quasicrystalline transmission line, we must present the background for modeling transmission lines in general. Consider a superconducting (lossless) transmission-line resonator with capacitance $c(x)$ per unit length and inductance $\ell(x)$ per unit length. The transmission-line resonator is coupled by capacitors with capacitances C_L and C_R on the left and right to the circuits L and R, respectively. The generalized flux $\phi(x,t)$ is defined as

$$\phi(x,t) = \int_{-\infty}^{t} V(x,t')\,\mathrm{d}t' \tag{2.1}$$

where $V(x,t)$ is the voltage at position x along the transmission line at time t. The system may be modeled as the continuum limit of N coupled LC circuits, with the jth circuit having capacitance $c_j\,\mathrm{d}x$ and inductance $\ell_j\,\mathrm{d}x$. The total length of the transmission line is

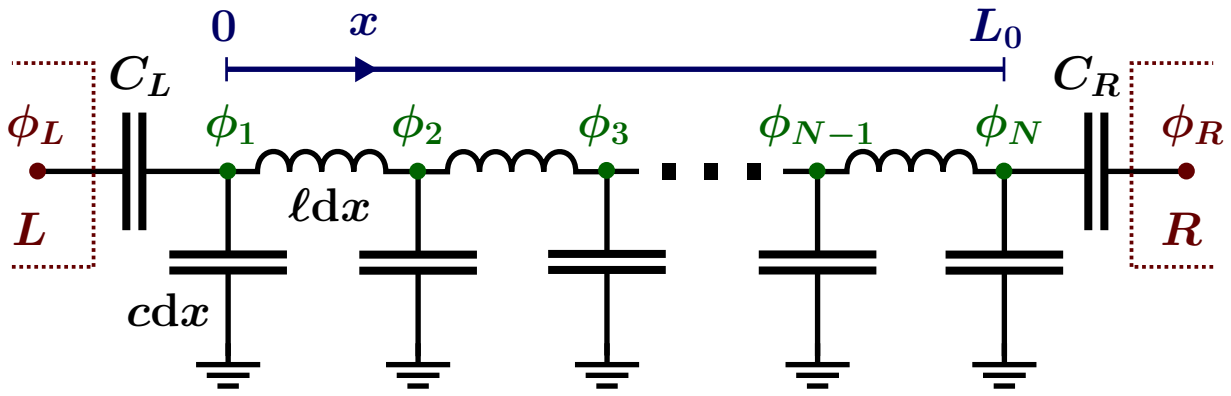

Figure 2.1: Circuit diagram of a discretized transmission-line resonator. A transmission-line resonator of length L_0, capacitance per unit length c, and inductance per unit length ℓ may be discretized into a chain of coupled LC circuits, with the jth circuit having capacitance $c_j\,\mathrm{d}x$ and inductance $\ell_j\,\mathrm{d}x$. The coordinate x labels the position along the transmission line. The transmission line is coupled to ϕ_L of the circuit to the left through a capacitor of capacitance C_L and to ϕ_R of the circuit to the right through a capacitor of capacitance C_R. (Figure from Andy C.Y. Li.)

$L_0 = N\,\mathrm{d}x$. In the discretized form, the full system Lagrangian is given by

$$\mathcal{L} = \mathcal{L}'_L + \mathcal{L}'_R + \frac{C_L}{2}\left(\dot{\phi}_1 - \dot{\phi}_L\right)^2 + \frac{C_R}{2}\left(\dot{\phi}_N - \dot{\phi}_R\right)^2 + \sum_{j=1}^{N}\frac{c_j\,\mathrm{d}x}{2}\dot{\phi}_j^2 - \sum_{j=2}^{N}\frac{1}{2\ell_j\,\mathrm{d}x}\left(\phi_j - \phi_{j-1}\right)^2 \tag{2.2}$$

where $\mathcal{L}'_L$ and $\mathcal{L}'_R$ are the Lagrangians of the left and right circuits respectively. We write this Lagrangian as the sum of four terms:

$$\mathcal{L} = \mathcal{L}_L + \mathcal{L}_R + \mathcal{L}_{\mathrm{coup}} + \mathcal{L}_{\mathrm{TL}} \tag{2.3}$$

where $\mathcal{L}_L = \mathcal{L}'_L + C_L\dot{\phi}_L^2/2$ and $\mathcal{L}_R = \mathcal{L}'_R + C_R\dot{\phi}_R^2/2$ are the Lagrangians for the left and right circuits, respectively, with the addition terms due to capacitive coupling with the transmission line. The term $\mathcal{L}_{\mathrm{coup}} = -C_L\dot{\phi}_L\dot{\phi}_1 - C_R\dot{\phi}_N\dot{\phi}_R$ refers to the coupling between the transmission line and the circuits. The last term, the Lagrangian of the transmission line, is

the most important:

$$\mathcal{L}_{\mathrm{TL}} = \frac{C_L}{2}\dot{\phi}_1^2 + \frac{C_R}{2}\dot{\phi}_N^2 + \sum_{j=1}^{N}\frac{c_j\,\mathrm{d}x}{2}\dot{\phi}_j^2 - \sum_{j=2}^{N}\frac{1}{2\ell_j}\left(\frac{\phi_j - \phi_{j-1}}{\mathrm{d}x}\right)^2 \mathrm{d}x\,. \tag{2.4}$$

In the continuum limit, we have $N \to \infty$ and $\mathrm{d}x \to 0$, but $N\,\mathrm{d}x = L_0$ is constant so that the sums become integrals. In addition, the discrete functions for flux, capacitance per unit length, and inductance per unit length turn into continuous functions of distance along the transmission line: $\phi_j(t) \to \phi(x,t)$, $c_j \to c(x)$, and $\ell_j \to \ell(x)$. The Lagrangian for the transmission line is now

$$\mathcal{L}_{\mathrm{TL}} = \frac{C_L}{2}\left(\left.\frac{\partial\phi}{\partial t}\right|_{x=0}\right)^2 + \frac{C_R}{2}\left(\left.\frac{\partial\phi}{\partial t}\right|_{x=L_0}\right)^2 + \int_0^{L_0}\frac{c(x)}{2}\left(\frac{\partial\phi}{\partial t}\right)^2\mathrm{d}x - \int_0^{L_0}\frac{1}{2\ell(x)}\left(\frac{\partial\phi}{\partial x}\right)^2\mathrm{d}x\,. \tag{2.5}$$

By using calculus of variations to impose that the action $S = \int \mathcal{L}\,\mathrm{d}t$ is stationary, we obtain an equation of motion in addition to boundary conditions for the ends of the transmission line:

$$c(x)\frac{\partial^2\phi}{\partial t^2} = \frac{\partial}{\partial x}\left(\frac{1}{\ell(x)}\frac{\partial\phi}{\partial x}\right), \tag{2.6}$$

$$\left.\frac{\partial\phi}{\partial x}\right|_{x=0} = \ell(0)C_L\left.\frac{\partial^2\phi}{\partial t^2}\right|_{x=0}, \tag{2.7}$$

$$\left.\frac{\partial\phi}{\partial x}\right|_{x=L_0} = -\ell(L_0)C_R\left.\frac{\partial^2\phi}{\partial t^2}\right|_{x=L_0}. \tag{2.8}$$

To solve for the eigenmodes, we use separation of variables with

$$\phi(x,t) = \varphi(x)e^{-i\omega t} \tag{2.9}$$

where ω is an eigenfrequency. The equation of motion and boundary conditions are then given by

$$\frac{\mathrm{d}}{\mathrm{d}x}\left(\frac{1}{\ell(x)}\frac{\mathrm{d}\varphi(x)}{\mathrm{d}x}\right) = -c(x)\omega^2\varphi(x), \tag{2.10}$$

$$\left.\frac{\mathrm{d}\varphi}{\mathrm{d}x}\right|_{x=0} = -\ell(0)C_L\omega^2\varphi(0), \tag{2.11}$$

$$\left.\frac{\mathrm{d}\varphi}{\mathrm{d}x}\right|_{x=L_0} = \ell(L_0)C_R\omega^2\varphi(L_0). \tag{2.12}$$

Note that if $c(x)$ and $\ell(x)$ were independent of position, then Eq. (2.6) would become a wave equation, and Eq. (2.10) would have sinusoidal solutions. We will make use of this point in Section 2.2.

2.2 Chains of Resonators

We will now develop the mathematical formalism for a transmission-line resonator Fibonacci quasicrystal. Consider a transmission line that has N sections, which we call resonators, with the nth section of length L_n. The capacitance c_n and inductance ℓ_n per unit length within each resonator are constant, but we allow them to vary from resonator to resonator. We can also exchange these variables for the wave speed $v_n = 1/\sqrt{c_n\ell_n}$ and characteristic impedance $z_n = \sqrt{\ell_n/c_n}$ in each section. Independently varying wave speeds and impedances is how we will construct our Fibonacci quasicrystal. (However, precisely how the v_n and z_n vary does not concern us in this section.) The spatial dependence of the flux $\varphi_n(x_n)$ in the nth resonator then obeys

$$\frac{\mathrm{d}^2\varphi_n}{\mathrm{d}x_n^2} = -c_n\ell_n\omega^2\varphi_n(x_n) \tag{2.13}$$

so the solution is

$$\varphi_n(x_n) = A_n \sin\left(\frac{\omega x_n}{v_n}\right) + B_n \cos\left(\frac{\omega x_n}{v_n}\right) \tag{2.14}$$

where $x_n \in [0, L_n]$ is the spatial coordinate and the coefficients A_n and B_n are determined by boundary conditions. The flux must be continuous across different sections, but its first derivative is discontinuous if the inductance per unit length varies:

$$\varphi_n(L_n) = \varphi_{n+1}(0), \tag{2.15}$$

$$\frac{1}{\ell_n}\left.\frac{\mathrm{d}\varphi_n}{\mathrm{d}x_n}\right|_{x_n=L_n} = \frac{1}{\ell_{n+1}}\left.\frac{\mathrm{d}\varphi_{n+1}}{\mathrm{d}x_{n+1}}\right|_{x_{n+1}=0}. \tag{2.16}$$

The condition on the first derivative is equivalent to contintuity of the current. In addition, there are still the boundary conditions for the ends of the transmission line, which now take the form

$$\left.\frac{\mathrm{d}\varphi_1}{\mathrm{d}x_1}\right|_{x_1=0} = -\ell_1 C_L \omega^2 \varphi_1(0), \tag{2.17}$$

$$\left.\frac{\mathrm{d}\varphi_N}{\mathrm{d}x_N}\right|_{x_N=L_N} = \ell_N C_R \omega^2 \varphi_N(L_N). \tag{2.18}$$

Imposing the boundary conditions in Eqs. (2.15) and (2.16) to the solution in Eq. (2.14) yields the following matrix equation:

$$\begin{pmatrix} A_{n+1} \\ B_{n+1} \end{pmatrix} = \begin{pmatrix} \frac{z_{n+1}}{z_n}\cos\left(\frac{\omega L_n}{v_n}\right) & -\frac{z_{n+1}}{z_n}\sin\left(\frac{\omega L_n}{v_n}\right) \\ \sin\left(\frac{\omega L_n}{v_n}\right) & \cos\left(\frac{\omega L_n}{v_n}\right) \end{pmatrix} \begin{pmatrix} A_n \\ B_n \end{pmatrix} \equiv M_n \begin{pmatrix} A_n \\ B_n \end{pmatrix}. \tag{2.19}$$

The transfer matrix method may be employed to determine a relation between A_1, B_1, A_N, and B_N:

$$\begin{pmatrix} A_N \\ B_N \end{pmatrix} = M_{N-1} M_{N-2} \dots M_2 M_1 \begin{pmatrix} A_1 \\ B_1 \end{pmatrix}. \tag{2.20}$$

For simplicity, we define $M \equiv M_{N-1} M_{N-2} \dots M_2 M_1$, which is represented as

$$M = \begin{pmatrix} M_{11} & M_{12} \\ M_{21} & M_{22} \end{pmatrix}. \tag{2.21}$$

Eq. (2.20) along with Eqs. (2.17) and (2.18) give a linear system of four equations for A_1, B_1, A_N, and B_N. In matrix form, this system of equations can be written as

$$\begin{pmatrix} M_{11} & M_{12} & -1 & 0 \\ M_{21} & M_{22} & 0 & -1 \\ 1 & z_1 C_L \omega & 0 & 0 \\ 0 & 0 & z_N C_R \omega \sin\left(\frac{\omega L_N}{v_N}\right) - \cos\left(\frac{\omega L_N}{v_n}\right) & z_N C_R \omega \cos\left(\frac{\omega L_N}{v_N}\right) + \sin\left(\frac{\omega L_N}{v_N}\right) \end{pmatrix} \begin{pmatrix} A_1 \\ B_1 \\ A_N \\ B_N \end{pmatrix} = 0. \tag{2.22}$$

Because we are interested in nontrivial solutions for the A_n and B_n coefficients, the determinant of the 4×4 matrix above must vanish. The eigenfrequencies are thus positive solutions to the equation

$$d(\omega) \equiv \begin{vmatrix} M_{11} & M_{12} & -1 & 0 \\ M_{21} & M_{22} & 0 & -1 \\ 1 & z_1 C_L \omega & 0 & 0 \\ 0 & 0 & z_N C_R \omega \sin\left(\frac{\omega L_N}{v_N}\right) - \cos\left(\frac{\omega L_N}{v_n}\right) & z_N C_R \omega \cos\left(\frac{\omega L_N}{v_N}\right) + \sin\left(\frac{\omega L_N}{v_N}\right) \end{vmatrix} = 0. \tag{2.23}$$

For a given eigenfrequency, by the third line in Eq. (2.22), we have

$$A_1 = -z_1 C_L \omega B_1. \tag{2.24}$$

Thus, if $B_1 = 0$, then we must also have $A_1 = 0$, and by the transfer matrix method, $A_n = B_n = 0$ for all n, rendering the solution for $\varphi(x)$ trivial. Hence, to obtain a nontrivial solution, we must certainly have $B_1 \neq 0$. Since we are free to choose the normalization for the eigenmodes, we can set $B_1 = 1$ in numerical calculations. Then we can determine A_1 by using Eq. (2.24), and the rest of the A_n and B_n may be computed with the transfer matrix method.

Chapter 3

Quasiperiodic Impedances, Constant Speeds

We next discuss results obtained by applying the methods from the previous chapter numerically. In this section, we consider $N = 1000$ resonators with impedances that vary in the pattern of a Fibonacci quasicrystal. (Since 1000 is not a Fibonacci number, we simply truncate the pattern of the Fibonacci quasicrystal after 1000 units.) The two possible impedances are $z_1 = 1$ and $z_2 = 0.25$. We take $L_n = 1$ and $v_n = 1$ for all n as well as $C_R = C_L = 1$.

We plot $d(\omega)$ to observe the structure of the eigenfrequencies. The functional form of $d(\omega)$ is not relevant, but its zeros are the eigenfrequencies. While there are infinitely many of these eigenfrequencies, we are generally concerned with the lowest ones. Self-similarity in the structure of the eigenfrequencies is not clear from the plots, but we can observe a hierarchy of gaps. There are smaller gaps in the spectrum in between larger gaps, which should be present if the spectrum is self-similar. In Figure 3.1, the interval $4.6 < \omega < 4.8$ appears to be a continuous band in the frequency spectrum. However, upon a closer look in Figure 3.2, we see that there are gaps in this interval that are much smaller than the ones the appear in Figure 3.1. We observe similar results for the interval $4.705 < \omega < 4.720$ in Figure 3.3. This

is consistent with the structure of the eigenvalue spectrum of other Fibonacci quasicrystals.

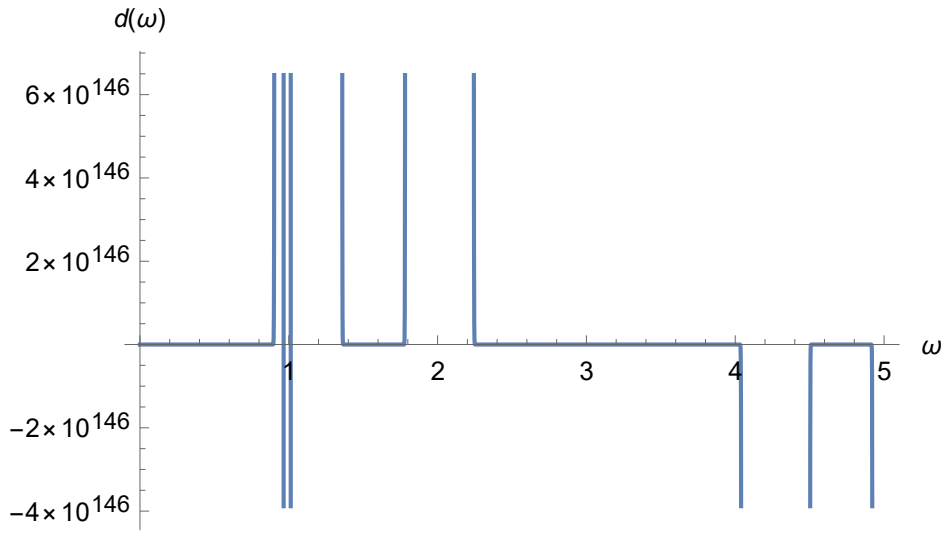

Figure 3.1: The function $d(\omega)$ for $0 < \omega < 5$. The zeros of $d(\omega)$ are the eigenfrequencies.

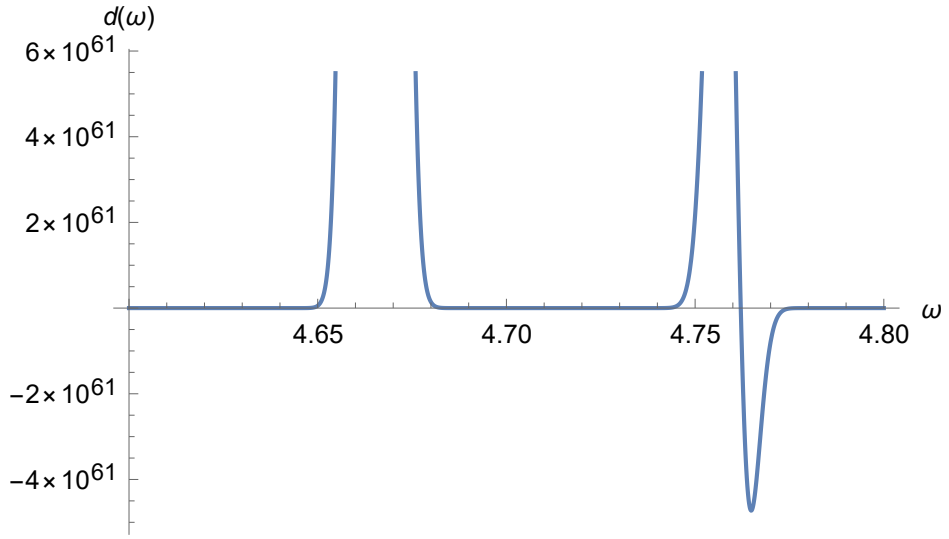

Figure 3.2: The function $d(\omega)$ for $4.6 < \omega < 4.8$. This region of frequencies looks like it contains no gaps in Figure 3.1, but the smaller gaps are visible in this plot.

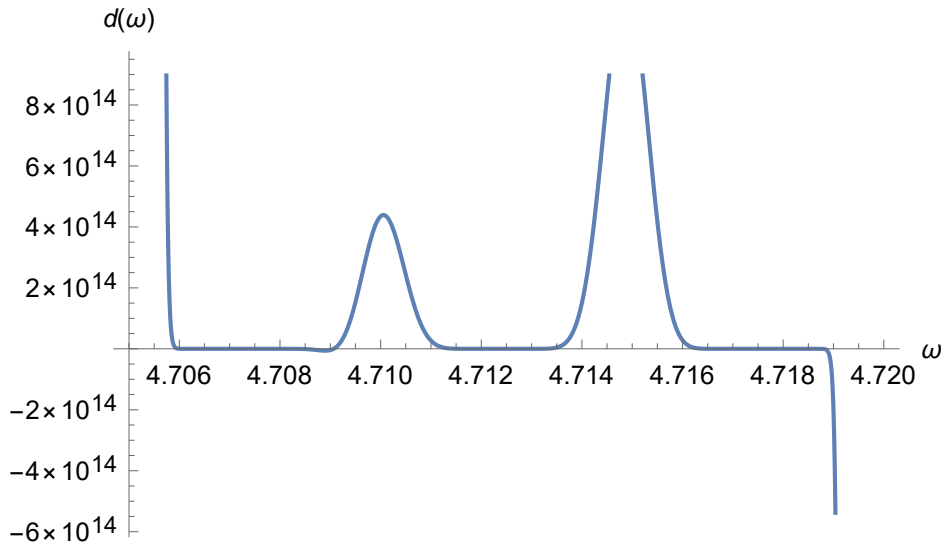

Figure 3.3: The function $d(\omega)$ for $4.705 < \omega < 4.720$. The gaps in this plot are too small to be visible in Figure 3.1 or Figure 3.2.

The eigenmodes are similar to those obtained in the mass-spring system. The high-frequency modes (Figure 3.4) have a fractal structure but not the low-frequency modes, which are much more delocalized (Figure 3.5). Modes of extremely low frequency look sinusoidal (Figure 3.6). These results suggest that the transmission-line quasicrystal with varying impedances have preserved the expected properties of Fibonacci quasicrystals.

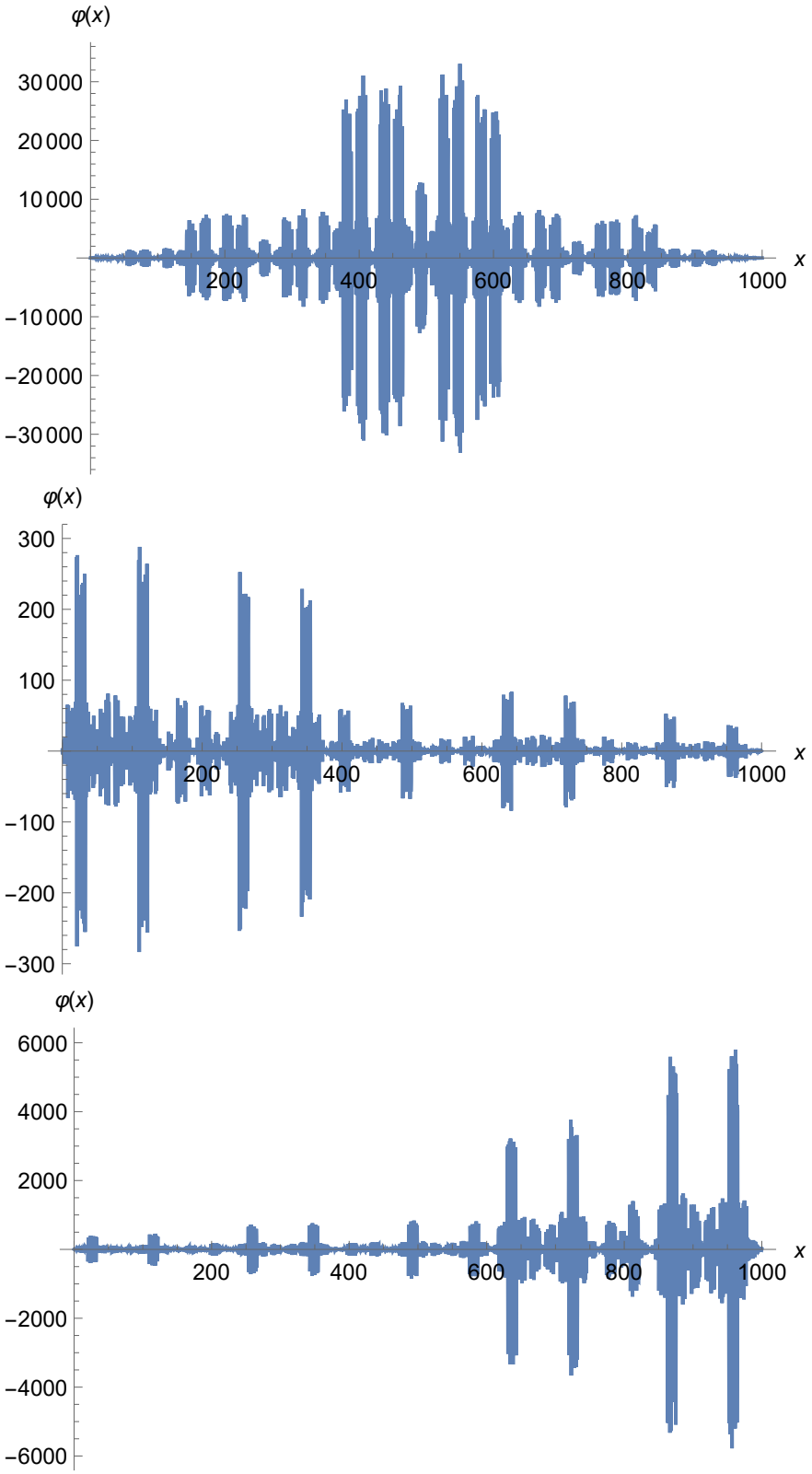

Figure 3.4: Eigenmodes for $N = 1000$ resonators with eigenfrequencies 4.82294, 4.79969, and 4.60014, respectively. These eigenmodes display the self-similarity that is characteristic of a quasicrystal.

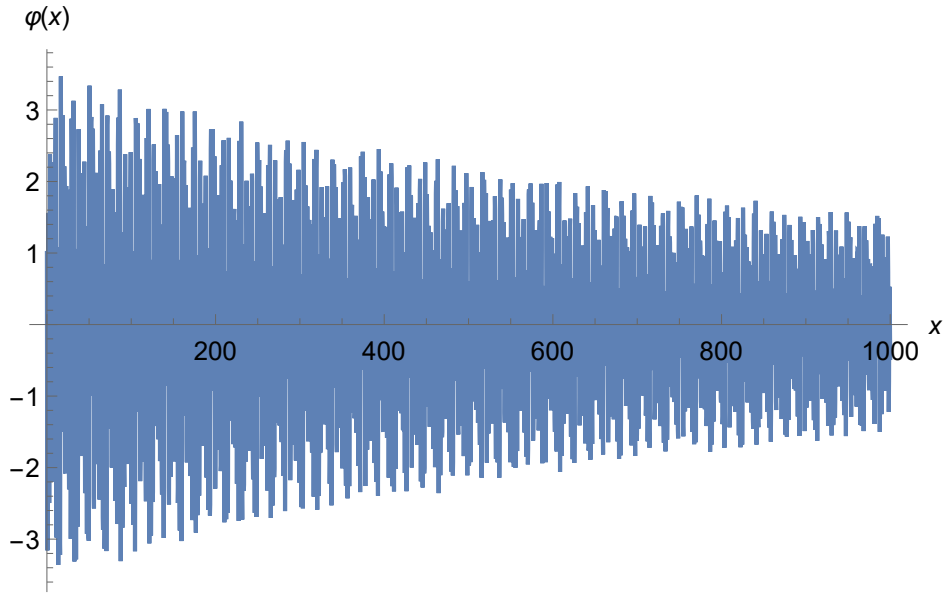

Figure 3.5: Eigenmode for $N = 1000$ resonators with eigenfrequency $\omega = 2.99987$. Self-similarity is not present in this delocalized lower-frequency mode.

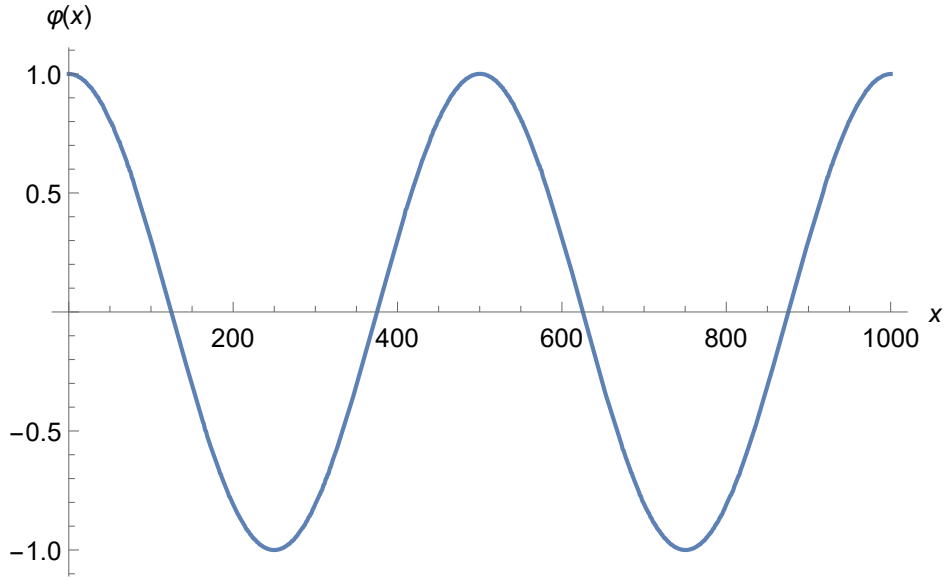

Figure 3.6: Eigenmode for $N = 1000$ resonators with eigenfrequency $\omega = 0.0101454$. The low-frequency eigenmode looks like a sinusoidal wave.

Chapter 4

KKT Renormalization-Group Analysis

We now introduce another method to compute the eigenfrequencies discovered by Kohmoto, Kadanoff, and Tang (KKT), which they develop for a tight-binding model [10]. We apply their method to our Fibonacci quasicrystal of resonators. In previous sections, we approximated the quasicrystal's behavior by examining systems composed of a large number of resonators. In this section, we use a periodic approximation: an infinite transmission line with infinitely many resonators that repeat a finite portion of the Fibonacci pattern periodically. Let this portion be of length F_m where F_m is the mth Fibonacci number. Thus, the problem is periodic with period F_m. The method of KKT requires transfer matrices that have unit determinant. In our case, we have $\det(M_n) = z_{n+1}/z_n$ [see Eq. (2.19)]. However, we can transform the coefficients according to

$$\begin{pmatrix} \tilde{A}_n \\ \tilde{B}_n \end{pmatrix} = \frac{1}{\sqrt{z_n}} \begin{pmatrix} A_n \\ B_n \end{pmatrix}. \tag{4.1}$$

This scaling of the coefficients transforms the transfer matrix M_n to

$$\tilde{M}_n = \sqrt{\frac{z_n}{z_{n+1}}} M_n = \begin{pmatrix} \sqrt{\frac{z_{n+1}}{z_n}} \cos\left(\frac{\omega L}{v_n}\right) & -\sqrt{\frac{z_{n+1}}{z_n}} \sin\left(\frac{\omega L}{v_n}\right) \\ \sqrt{\frac{z_n}{z_{n+1}}} \sin\left(\frac{\omega L}{v_n}\right) & \sqrt{\frac{z_n}{z_{n+1}}} \cos\left(\frac{\omega L}{v_n}\right) \end{pmatrix}, \tag{4.2}$$

which does in fact have unit determinant. We have assumed that the length of each resonator is the same: $L_n = L$ for all n. We define the transfer matrix P_l for a Fibonacci number of steps by

$$P_l \equiv \tilde{M}_{F_l} \tilde{M}_{F_l - 1} \ldots \tilde{M}_2 \tilde{M}_1 \tag{4.3}$$

where F_l is the lth Fibonacci number. For these matrices P_l, the following recursion relation holds due to the pattern of the Fibonacci quasicrystal:

$$P_{l+1} = P_{l-1} P_l. \tag{4.4}$$

The relation is valid because the Fibonacci quasicrystal of length $l+1$ may be constructed by adding the pattern of the Fibonacci quasicrystal of length $l-1$ to the end of the quasicrystal of length l. Eq. (4.4) implies that

$$P_{l+1} + P_{l-2}^{-1} = P_{l-1} P_l + P_{l-1} P_l^{-1}. \tag{4.5}$$

Taking the trace of this equation, we find a recursion relation for $x_l \equiv \mathrm{tr}(P_l)/2$:

$$x_{l+1} = 2 x_l x_{l-1} - x_{l-2}. \tag{4.6}$$

Eq. (4.6) requires that P_l is a 2×2 matrix with $\det(P_l) = 1$ for each l so that $\mathrm{tr}(P_l) I = P_l + P_l^{-1}$ by the Cayleigh-Hamilton theorem. (Here, I is the identity matrix.) In addition

to Eq. (4.6), we have the initial conditions

$$x_2 = \cos\left(\frac{\omega L}{v_1}\right)\cos\left(\frac{\omega L}{v_2}\right) - \frac{1}{2}\left(\frac{z_1}{z_2} + \frac{z_2}{z_1}\right)\sin\left(\frac{\omega L}{v_1}\right)\sin\left(\frac{\omega L}{v_2}\right), \tag{4.7}$$

$$x_1 = \cos\left(\frac{\omega L}{v_1}\right), \tag{4.8}$$

$$x_0 = \cos\left(\frac{\omega L}{v_2}\right). \tag{4.9}$$

These initial conditions together with Eq. (4.6) may be used to determine $x_m = x_m(\omega)$. If $|x_m(\omega)| \leq 1$, then ω is an eigenfrequency. If $|x_m(\omega)| > 1$, then ω cannot be an eigenfrequency since the solution would be unbounded.

4.1 Closing the Gaps: Constant Impedances

Suppose the impedances are all the same across the transmission line, but the speeds vary in the pattern of a Fibonacci quasicrystal. Then each transfer matrix takes the form

$$\tilde{M}_n = M_n = \begin{pmatrix} \cos\left(\frac{\omega L}{v_n}\right) & -\sin\left(\frac{\omega L}{v_n}\right) \\ \sin\left(\frac{\omega L}{v_n}\right) & \cos\left(\frac{\omega L}{v_n}\right) \end{pmatrix}. \tag{4.10}$$

Note that $M_n \in SO(2)$ is a rotation matrix, so for any arbitrary product of such matrices, the angles simply add:

$$P_m = M_{F_m} M_{F_m - 1} \ldots M_1 = \begin{pmatrix} \cos\left(\sum_{n=1}^{F_m} \frac{\omega L}{v_n}\right) & -\sin\left(\sum_{n=1}^{F_m} \frac{\omega L}{v_n}\right) \\ \sin\left(\sum_{n=1}^{F_m} \frac{\omega L}{v_n}\right) & \cos\left(\sum_{n=1}^{F_m} \frac{\omega L}{v_n}\right) \end{pmatrix}. \tag{4.11}$$

Therefore, we have

$$|x_m(\omega)| = \left|\cos\left(\sum_{n=1}^{F_m} \frac{\omega L}{v_n}\right)\right| \leq 1 \tag{4.12}$$

for *any* value of ω. Hence, any $\omega > 0$ is an allowed eigenfrequency. This suggests that the system becomes gapless in this special case. To show that this conclusion agrees with our method of determining eigenfrequencies as the zeros of $d(\omega)$ [Eq. (2.23)], we numerically compute $d(\omega)$ for various numbers of resonators. As the number of resonators increases, the spacing between the zeros of $d(\omega)$ decreases, as expected (see Figure 4.2). For these calculations, we consider $N = 1000$ resonators, and the two possible wave speeds are $v_1 = 1$ and $v_2 = 0.25$. We take $L_n = 1$ and $z_n = 1$ for all n as well as $C_R = C_L = 1$.

A gapless eigenvalue spectrum is not consistent with other systems of quasicrystals that we have previously observed, so it is natural to ask whether any other characteristics typical of quasicrystals are preserved for this system. From the plots in Figure 4.1, we see that self-similarity of eigenmodes is not present. The amplitude for a given eigenmode remains the same across all resonators precisely because M_n in Eq. (4.10) is a rotation matrix so that $\sqrt{A_n^2 + B_n^2} = \sqrt{A_{n+1}^2 + B_{n+1}^2}$. We can still, however, observe that the wavelength varies across resonators in the pattern of a Fibonacci quasicrystal, which follows directly from Eq. (2.14).

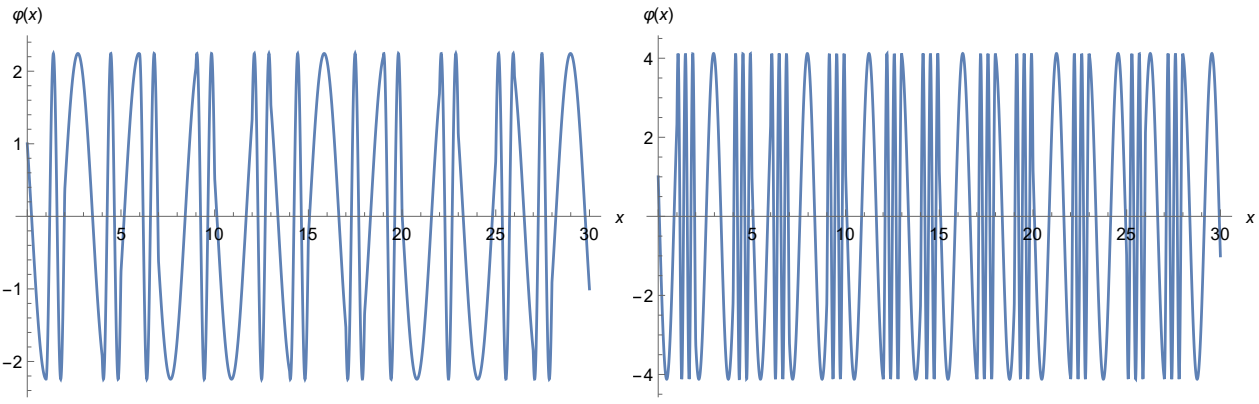

Figure 4.1: Eigenmodes for $N = 30$ resonators for varied wave speeds and constant impedances. The eigenmode depicted in the top plot has frequency 2.0001, and the eigenmode pictured in the bottom plot has frequency 3.99710. While these eigenmodes do not show self-similarity, their wavelengths follow the pattern of the Fibonacci quasicrystal across resonators.

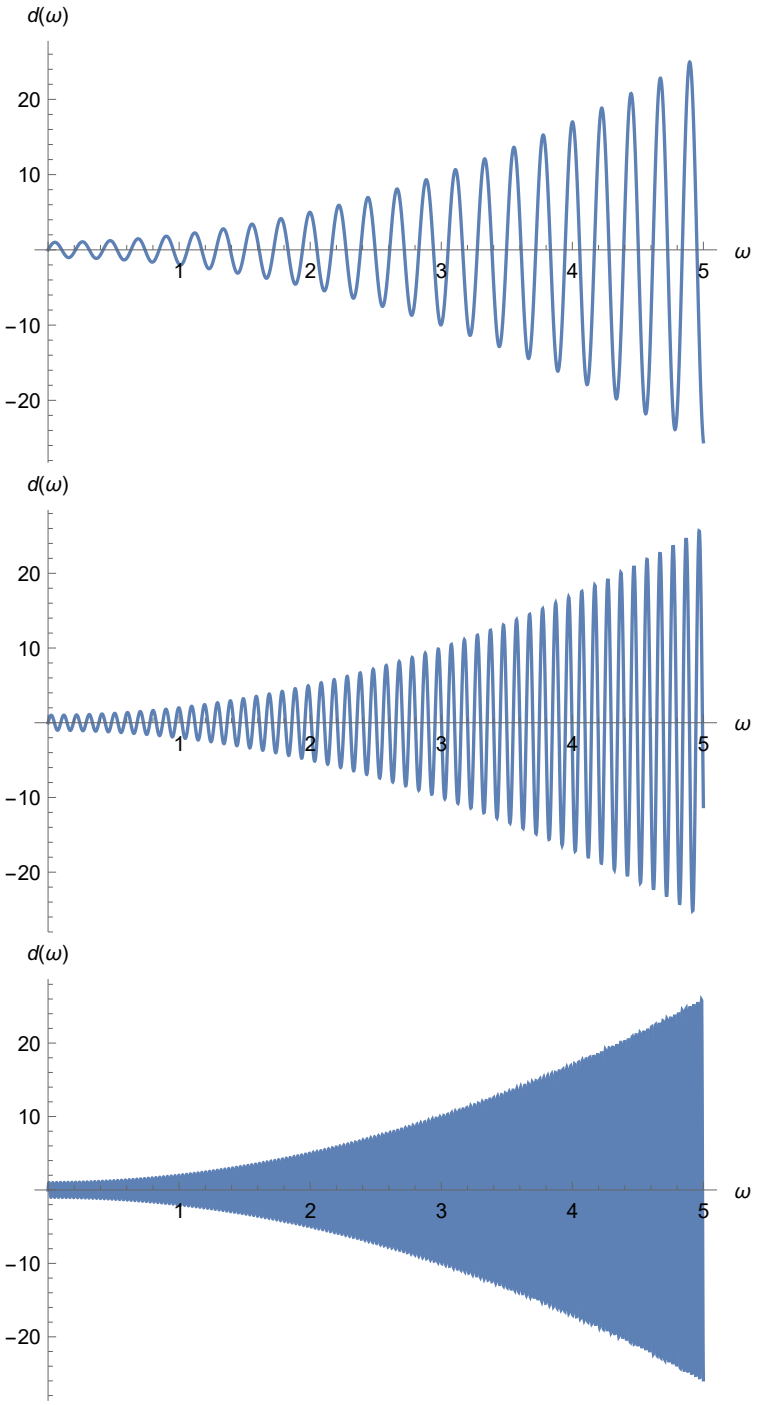

Figure 4.2: The function $d(\omega)$ for 13, 30, and 100 resonators, respectively. The zeros of $d(\omega)$ are the eigenfrequencies. As the number of resonators increases, the spacing between the eigenfrequencies decreases.

4.2 KKT Invariant

By using the recursion relation in Eq. (4.6), KKT also found an associated invariant λ:

$$\lambda^2 = -1 + x_l^2 + x_{l-1}^2 + x_{l-2}^2 - 2x_l x_{l-1} x_{l-2}. \tag{4.13}$$

The quantity λ does not depend on l, which may be easily verified by direct substitution using Eq. (4.6). By applying this analysis to the transmission-line system, we obtain a general expression for the invariant due to the initial conditions:

$$\lambda^2 = \frac{1}{4}\left(\frac{z_1}{z_2} - \frac{z_2}{z_1}\right)^2 \sin\left(\frac{\omega L}{v_1}\right)\sin\left(\frac{\omega L}{v_2}\right). \tag{4.14}$$

For the special case that the impedances are all constant, we find that $\lambda = 0$. If the wave speeds are all constant but the impedances vary in the pattern of a Fibonacci quasicrystal, then

$$\lambda = \frac{1}{2}\left|\left(\frac{z_1}{z_2} - \frac{z_2}{z_1}\right)\sin\left(\frac{\omega L}{v_1}\right)\right| = \frac{\left|(z_1^2 - z_2^2)\sin\left(\frac{\omega L}{v_1}\right)\right|}{2z_1 z_2}. \tag{4.15}$$

This generalizes the KKT formalism and invariant to our systems of transmission-line quasicrystals.

Chapter 5

Conclusions

The work in this thesis has shown how to mathematically model a new artificial Fibonacci quasicrystal constructed of transmission-line resonators. Numerical calculations with this model were used to study two types of quasicrystals that can be constructed with resonators. In the case of varying impedances and constant speeds, we provided examples in which the typical properties of quasicrystals are present, namely the hierarchy of gaps in the eigenfrequency spectrum and self-similarity of high-frequency eigenmodes. In examining the quasicrystal in which wave speeds vary while impedances are constant, we observed that the frequency spectrum is gapless. Moreover, the eigenmodes have constant amplitude but have wavelengths that vary according to the Fibonacci quasicrystal sequence. We were able to understand these results by extending the KKT renormalization-group method. This method is associated with an invariant, which we computed for our quasicrystal of resonators.

Bibliography

[1] D. Monroe. *Focus: Nobel Prize–discovery of quasicrystals*, Phys. Rev. Focus **28**, 14 (2011).

[2] D. L. D. Caspar and E. Fontano, *Five-fold symmetry in crystalline quasicrystal lattices*, Proc. Natl. Acad. Sci. **93**, 14271-14278 (1996).

[3] M. Kohmoto, B. Sutherland, and C. Tang, *Critical wave functions and a Cantor-set spectrum of a one-dimensional quasicrystal model*, Phys. Rev. B **35**, 1020 (1987).

[4] Y. E. Kraus and O. Zilberberg, *Topological equivalence between the Fibonacci quasicrystal and the Harper model*, Phys. Rev. Lett. **109**, 116404 (2012).

[5] Y. E. Kraus, Z. Ringel, and O. Zilberberg, *Four-dimensional quantum Hall effect in a two-dimensional quasicrystal*, Phys. Rev. Lett. **111**, 226401 (2013).

[6] K. Singh, K. Saha, S. A. Parameswaran, and D. M. Weld, *Fibonacci optical lattices for tunable quantum quasicrystals*, Phys. Rev. A **92**, 063426 (2015).

[7] M. Verbin, O. Zilberberg, Y. Lahini, Y. E. Kraus, and Y. Silberberg, *Topological pumping over a photonic Fibonacci quasicrystal*, Phys. Rev. B **91**, 064201 (2015).

[8] B. N. Parlett, *The Symmetric Eigenvalue Problem*, Prentice Hall, Inc. (1980).

[9] A. A. Houck, J. Türeci, and Jens Koch, *On-chip quantum simulation with superconducting circuits*, Nat. Phys. **8**, 292 (2012).

[10] M. Kohmoto, L. Kadanoff, and C. Tang, *Localization problem in one dimension: mapping and escape*, Phys. Rev. Lett. **50**, 1870 (1983).